Journal of Functional Foods 35 (2017) 352–362

Contents lists available at ScienceDirect

Journal of Functional Foods

journal homepage: www.elsevier.com/locate/jff

Structural characterization and immunomodulatory activity of novel polysaccharides from *Citrus aurantium* Linn. variant *amara* Engl

Chun-Yan Shen [a], Jian-Guo Jiang [a,*], Ming-Qiang Li [b,c], Chao-Yang Zheng [b], Wei Zhu [b,*]

[a] College of Food and Bioengineering, South China University of Technology, Guangzhou 510640, China
[b] The Second Affiliated Hospital, Guangzhou University of Chinese Medicine, Guangzhou 510120, China
[c] Sci-tech Industrial Park, Guangzhou University of Chinese Medicine, Guangzhou 510120, China

ARTICLE INFO

Article history:
Received 24 February 2017
Received in revised form 20 May 2017
Accepted 25 May 2017
Available online 5 June 2017

Keywords:
Polysaccharide
Citrus aurantium L. var. *amara* Engl.
Structure
Immunomodulatory activity
MAPK
NF-κB

ABSTRACT

Two polysaccharides CAVAP-I and CAVAP-II from *Citrus aurantium* L. var. *amara* Engl showed significant structural differences. Average molecular weights of CAVAP-I and CAVAP-II were 10.5 kDa and 4.5 kDa. Triple-helix conformation existed in CAVAP-II rather than CAVAP-I. Arabinose, mannose, glucose and galactose formed main components of CAVAP-I and CAVAP-II at different ratios. (1 → 3,6)-β-D-Gal and (1 → 5)-α-L-Ara composed the backbone of CAVAP-I and CAVAP-II. CAVAP-II displayed greater immune enhancement potential than CAVAP-I. CAVAP-II significantly promoted interleukin-6 (IL-6) and tumor necrosis factor-α (TNF-α) production, and inducible nitric oxide synthase, IL-6, TNF-α and interleukin-1 beta mRNA expression by activating phosphorylated extracellular signal-regulated kinase, c-Jun N-terminal kinase, P38 and P65. These results indicated that structures were closely related to immunomodulatory activity of polysaccharides. CAVAP-II showed the greatest immunostimulation potential followed by CAVAP-I and CAVAPs by activating mitogen-activated protein kinase (MAPK) and nuclear factor-kappa B (NF-κB) pathways.

1. Introduction

Macrophages, playing central roles in the innate and adaptive immune responses, could protect the host by promoting production of numerous biologically active molecules that regulate the activity of other cells. Specifically, macrophages expressed inducible nitric oxide synthase (iNOS) upon activated with microbial or cytokine stimuli, which led to the secretion of nitric oxide (NO) from L-arginine. NO not only acted as a mediator of the immune system, but also exerted other functions, such as neural signal transmission and control of blood pressure. Reportedly, mitogen-activated protein kinase (MAPK) and nuclear factor-kappa B (NF-κB) signaling pathways were involved in the stimulation of various cytokines and chemokines thereby exerting the immune enhancement effects (Lu et al., 2015; Shen, Yang, Jiang, Zheng, & Zhu, 2017).

Natural products have been reported to exert pharmacological activities with few side effects (Zeng, Zao, Wang, Zhang, & Jiang, 2016). Of the ingredients in natural products, polysaccharides have been known as the major bioactive compounds possessing various bioactivities (Lu et al., 2015; Mao et al., 2016; Zhang et al., 2015). Especially, the immunomodulatory activity of polysaccharides was frequently reported (Fang et al., 2015; Kim et al., 2012; Lee et al., 2015). These literatures suggested that polysaccharides might be used as immunomodulators to help regulate or normalize the immune system. Furthermore, a growing number of published data focused on the structure–activity relationship of purified polysaccharides (Kakutani et al., 2007; Wang, Yang, Zhao, Lu, & Zhu, 2017; Wei et al., 2016; Zhang, Wang, Lai, & Wu, 2016). Reportedly, the structures related with immunomodulatory effects were proved to be the conformation, molecular weight, functional groups, monosaccharide composition, glycosidic-linkage and branching characteristics (Ferreira, Passos, Madureira, Vilanova, & Coimbra, 2015). Therefore, a basic understanding of primary structures of polysaccharides could lead to successful interpretation of their immunomodulatory activities.

Structural characterization and antioxidant activities of purified polysaccharides from *Citrus aurantium* L. (CAL) were reported by Wang et al. (2014). Furthermore, our previous study demonstrated that crude polysaccharides (CAVAPs) from blossoms of *Citrus aurantium* L. var. *amara* Engl. (CAVA) showed significant immune enhancement effect by activating the RAW264.7 (Shen et al., 2017). However, little information was available on the structural

* Corresponding authors.
E-mail addresses: cyshen0415@163.com (C.-Y. Shen), jgjiang@scut.edu.cn (J.-G. Jiang), limq0307@163.com (M.-Q. Li), cyzheng@163.com (C.-Y. Zheng), zhuwei9201@163.com (W. Zhu).

http://dx.doi.org/10.1016/j.jff.2017.05.055
1756-4646/

characteristics and immunomodulatory activities of purified polysaccharides from CAVA. Therefore, the objective of the current study was to gain insight into the structure–activity relationship of two novel polysaccharides isolated from CAVAPs. Initially, structure characterization of CAVAP-I as well as CAVAP-II, that might be responsible for the observed bioactivity, was compared. Furthermore, *in vitro* assays were designed to investigate the immunomodulatory activity of CAVAP-I and CAVAP-II on RAW264.7 cells, by determining the promoting effects on NO and cytokines, as well as the activation effects on MAPKs and NF-κB signaling pathways.

2. Materials and methods

2.1. Materials and chemicals

Citrus aurantium L. var. *amara* Engl. (CAVA), collected from Zhejiang Province of China, was purchased from Qingping traditional Chinese medicine market (Guangzhou, China). CAVAPs were extracted according to the method described by Shen et al. (2017). DEAE-52 cellulose and Sephadex G-100 were purchased from Beijing H&E Ltd. Corporation (Beijing, China). Myoinositol, standard monosaccharides (glucuronic acid, rhamnose, fucose, arabinose, xylose, mannose, glucose and galactose), Lipopolysaccharides (LPS) and 3-(4,5-Dimethyl-2-thiazolyl)-2,5-diphenyl-2H-tetrazolium bromide (MTT) were obtained from Sigma-Aldrich (Shanghai, China). Dulbecco's modified eagle medium (DMEM), fetal bovine serum (FBS), penicillin, streptomycin and trizol reagent were purchased from GIBCO (Grand Island, NY, USA). Mouse NO, interleukin-6 (IL-6) and tumor necrosis factor-α (TNF-α) detecting enzyme-linked immunosorbent assay (ELISA) kits were from Cusabio Biothch CO., Ltd. (Wuhan, China). The rabbit polyclonal GAPDH antibody, rabbit monoclonal phosphorylated extracellular signal-regulated kinase (ERK) antibody, rabbit monoclonal phosphorylated c-Jun N-terminal kinase (JNK) antibody, rabbit monoclonal phosphorylated P38 antibody, and rabbit monoclonal phosphorylated P65 antibody were all purchased from Cell Technology (Beverly, MA, USA). All of the other chemical reagents used in this study were analytical grade.

2.2. Extraction and purification of polysaccharides from blossoms of CAVA

CAVAPs were obtained according to our previous study (Shen, Zhang, & Jiang, 2017). Then, a total of 600 mg of CAVAPs was dissolved in 15 mL of distilled water, loaded onto the pre-equilibrated DEAE-Sepharose Fast Flow chromatography, and sequentially eluted with distilled water and 0.05 mol/L of NaCl aqueous solutions at a flow rate of 1.0 mL/min. Thereafter, the eluents were collected using an automated step-by-step fraction collector based on the phenol–sulfuric acid method, and then concentrated at 60 °C with a rotary vacuum evaporator. Two fractions (CAVAP-fr.1 and CAVAP-fr.2) were obtained after dialyzed (M_W cut off 8.0 kDa) and lyophilized. Moreover, Sephadex G-100 chromatography was used for further purification of CAVAP-fr.1 and CAVAP-fr.2. Briefly, 20 mg of each fraction was dissolved in 10 mL of distilled water and eluted with distilled water at a flow rate of 1.0 mL/min. The eluents were then collected and combined based on the phenol-sulfuric method. The resultant samples were named as CAVAP-I and CAVAP-II, respectively.

2.3. Structure characterization of homogeneous polysaccharides

2.3.1. Scanning electron microscope (SEM) analysis

CAVAP-I and CAVAP-II were coated with a thin layer of gold under reduced pressure and then examined with a field emission scanning electron microscope (JSM-5900LV, JEOL, Japan) at an accelerating voltage of 5.0 kV. The image magnifications were set as 500×, 1000× and 2000×.

2.3.2. Components analysis

Total sugar contents of CAVAP-I and CAVAP-II were determined by the modified phenol-sulfuric acid method and D-glucose was used as a standard to produce the calibration curve (Lu et al., 2015). Simultaneously, the contents of uronic acid were also detected at 520 nm using the carbozole and sulphuric acid method with glucuronic acid as a standard (Radhakrishnamurthy & Berenson, 1963). Furthermore, the protein levels were measured at 595 nm using Coomassie brilliant blue G-250 solutions and bovine serum albumin (BSA) was chosen as a standard (Bradford, 1976).

2.3.3. Molecular weight determination

Initially, CAVAP-I and CAVAP-II were diluted to 1 mg/mL and filtered through 0.22 μm microporous filtering films for future use. The molecular weights of CAVAP-I and CAVAP-II were performed on high performance gel permeation chromatography (HPGPC) (717Plus sample injector, 1525 pump; Waters) using a Waters HPLC system including a Waters TSK G-5000 PW × L TSK column, a G-3000 PW × L gel column and a Waters 2414 differential refractive index detector. Thereafter, the samples were eluted with 0.02 mol/L KH_2PO_4 (pH 6.0) solutions at a flow rate of 0.6 mL/min and dextrans of different molecular weights were used to obtain the calibration curve.

2.3.4. Infrared spectrum analysis

2 mg of CAVAP-I as well as CAVAP-II was ground to a fine powder and mixed with 200 mg of spectroscopic grade potassium bromide (KBr) powder, and then pressed into 1 mm pellets. Finally, the Fourier transform infrared (FT-IR) spectra were recorded in the 4000–400 cm^{-1} vibrations region with a Fourier transform infrared spectrophotometer (Bruker, Ettlingen, Germany) to investigate the organic functional groups.

2.3.5. Triple-Helix structure determination

The conformational structures of CAVAP-I and CAVAP-II were determined based on the Congo red method described as Lee et al. with minor modifications (Wang et al., 2016). Briefly, 5 mg of samples were initially prepared in 2 mL of distilled water and then mixed with 2 mL of Congo red (80 μmol/L) with vigorous stir. Furthermore, different NaOH solutions (0.1, 0.2, 0.3, 0.4 and 0.5 mol/L) were successively added to observe the evolution of maximum absorption wavelength (λ_{max}). Congo red solutions without samples in various NaOH concentrations were evaluated as the negative control.

2.3.6. Monosaccharide composition analysis

10 mg of CAVAP-I as well as CAVAP-II was hydrolyzed in 4 mL of 2 mol/L trifluoroacetic acid (TFA) for 6 h at 110 °C. A stream of nitrogen was used to seal the tested tubes. Acetylation was conducted based on the previous reports (Wang et al., 2017). Briefly, each sample was reacted with 10 mg of hydroxylamine hydrochloride and 1 mL of pyridine for 30 min at 90 °C. After cooling, 0.5 mL acetic anhydride was added and reacted for another 30 min at 90 °C. Thereafter, extraction was carried out three times with 1 mL of chloroform each time. The samples were dried and dissolved with chloroform and then filtered through a 0.22 μm filter. Then the acetate derivative products were analyzed by gas chromatography (GC) system fitted with a DP-1701 capillary column (30 m × 0.25 m × 0.25 μm) equipped with a flame ionization detector (FID). The procedures of GC were as follows: The heating program was increased from 180 to 220 °C at a speed of 2 °C/min

and kept at 220 °C for 1 min, then arose from 220 to 250 °C at a speed of 5 °C/min and remained at 250 °C for 5 min. The temperature of the FID detector was set at 300 °C, the column temperature was 190 °C and the injection volume was 10 μL. The standard monosaccharides including glucuronic acid, rhamnose, fucose, arabinose, xylose, mannose, glucose and galactose were also derivatized similarly to the treatment of CAVAP-I and CAVAP-II. Myoinositol was chosen as the interior reference.

2.3.7. Periodate oxidation-smith degradation analysis

25 mg of each sample was dissolved with ultrapure water and incubated in the dark at room temperature with 12.5 mL $NaIO_4$ (30 mmol/L) in a volumetric flask of 25 mL. The ultrapure water was added to make the constant volume, thereby resulting the final concentration of $NaIO_4$ (15 mmol/L). During the period of incubation, 0.1 mL of reaction solution was taken out at different time intervals including 0, 6, 12, 24, 30, 36, 48, 54, 60 and 72 h in order to detect the absorbance at 233 nm. When OD_{233} was constant, 2 mL of terminating agent (glycol) was added to stop the reaction. Then the consumption amount of $NaIO_4$ was determined according to the $NaIO_4$ standard curve. The resulting formic acid was quantified by titration with 0.01203 mol/L sodium hydroxide solution which was demarcated by potassium acid phthalate. Bromocresol blue was screened as indicator during titration. The remained samples were dialyzed in running water for 48 h and in distilled water for another 48 h. The resulting liquids were concentrated to about 10 mL, mixed with 70 mg sodium borohydride and reacted in the dark overnight to destroy the redundant furfural. Thereafter, the solutions obtained above were neutralized to pH 6.0–7.0 with 50% of acetic acid solutions. After dialysis in running water for 48 h and in distilled water for 48 h, the solutions were concentrated and dried. The dried residues were hydrolyzed with TFA and then acetylated with pyridine and hydroxylamine hydrochloride successively. Eventually, the acetate derivatives were analyzed using GC system with a DB-1701 capillary column (30 m × 0.25 m × 0.25 μm, 80–220 °C at 2 °C/min and then 220–250 °C at 5 °C/min). Glucuronic acid, rhamnose, fucose, arabinose, xylose, mannose, glucose, galactose, erythritol, glycol and glycerol were used as the standard substances.

2.3.8. Methylation analysis

Methylation analysis of CAVAP-I and CAVAP-II was conducted based on the reported method with slight modifications. About 10 mg of each sample was dissolved in 6 mL of anhydrous DMSO at 50 °C sonicated for 7 h until clear solutions were obtained. Then 120 mg of sodium hydroxide was added to the solutions and kept at 60 °C overnight. After adding 3.6 mL of methyl iodide with vigorous stirring for 1 h, the reaction was stopped by adding 6 mL of distilled water. The obtained solutions were then dialyzed against distilled water for 48 h at 4 °C. The methylated polysaccharides were extracted three times with dichloromethane and the resulting extracts were dried over sodium sulfate and eventually evaporated by a stream of nitrogen. Afterwards, the dried methylated polysaccharides (CAVAP-I and CAVAP-II) were hydrolyzed as described above. Then the hydrolysates were reduced by 70 mg of sodium borodeuteride and acetylated with 0.5 mL of acetic anhydride. Finally, the resultants were analyzed by GC coupled with MS system fitted with a HP-5 capillary column (30 nm × 0.25 mm × 0.25 μm, 150–180 °C at 10 °C/min, and then 180–260 °C at 15 °C/min) equipped with an ion trap MS detector.

2.3.9. NMR Spectroscopy analysis

CAVAP-I and CAVAP-II (50 mg) were dissolved with 0.8 mL D_2O in separate NMR tubes and then the ^{13}C NMR and ^{1}H NMR spectra were recorded on a Bruker 600 MHz NMR apparatus (AVANCE III HD 600, Bruker, USA).

2.4. Immunomodulatory activity

2.4.1. Cell culture

Mouse macrophage cell line RAW264.7, purchased from the cell bank of Shanghai of Chinese Academy of Sciences, were incubated at 37 °C in DMEM supplemented with 10% heat-inactivated FBS in a humidified atmosphere of 5% CO_2.

2.4.2. MTT assay for cell cytotoxicity

RAW264.7 cells in exponential growth phase, were adjusted to a concentration of 2×10^5 cells/mL and seeded onto the 96-well plate. After continuously incubation for 24 h, the cells were treated with CAVAP-I or CAVAP-II for 24 h at various concentrations of 16.13, 31.25, 62.5, 125, 200 and 250 μg/mL. Different concentrations of CAVAP-I and CAVAP-II were obtained by diluted in culture medium DMEM with half dilution method. The next day, the medium was discarded and 200 μL of MTT solution (0.5 mg/mL) diluted in DMEM was added to each well. After further incubation for an additional 4 h, the supernate was removed and 150 μL of DMSO was added to dissolve the produced formazan crystals. Eventually, the absorbance at 570 nm was measured using a microplate reader (Thermo Fisher Scientific, USA).

2.4.3. Measurement of NO and cytokines

RAW264.7 cells were loaded onto 24-well plates at 2×10^5 cells/well and administrated with CAVAP-I or CAVAP-II at different concentrations including 16.13, 31.25, 62.5, 125, 200 and 250 μg/mL for 24 h. After that, the supernatants of cells were collected. Nitrite accumulation was determined as an indicator of NO production with Griess reagent according to the published reports (Shen, Zhang, Zhang, & Jiang, 2016). Briefly, the harvested supernatants were mixed with an equal volume of Griess reagent A (1% sulphanilamide in 5% phosphoric acid) and Griess reagent B (0.1% N-1-naphtylethylenediamine dihydrochloride in distilled water), and then stood in the dark place at room temperature for 10 min. Afterwards, the absorbance at 540 nm was detected through a microplate reader. LPS (1 μg/mL) was used as the positive control. Furthermore, the secretion of IL-6 and TNF-α was determined by the commercially available ELISA kits.

2.4.4. RT-PCR analysis

RAW264.7 cells were seeded onto 6-well plates at the optimum density of 8×10^5 cells/well and incubated for 24 h prior to the sample treatment. Then, the supernates were removed and the cells were stimulated with CAVAP-II at different concentrations (125, 200 and 250 μg/mL). 24 h later, the cells were washed by cold phosphate-buffered saline (PBS) and the total RNA was extracted by the trizol reagent based on the manufactures' procedures. The isolated RNA was used for cDNA synthesis with reverse transcriptase. Then the cDNA encoding iNOS, IL-6, TNF-α and interleukine-1 beta (IL-1β) mRNA were quantified by RT-PCR analysis. GAPDH was used as the internal reference. The sequences of the specific primers were displayed in Table S1. The mRNA expression levels were expressed as the ratio of optimal density to GAPDH by calculating $^{\Delta\Delta}Ct$, and then analyzed using $2^{-\Delta\Delta}Ct$ method.

2.4.5. Western blotting analysis

Western blotting analysis was conducted according to the standard procedures published previously (Shen et al., 2017; Wang et al., 2017). Briefly, an aliquot of 2 mL RAW264.7 cells were seeded onto the 6-well plates at a concentration of 5×10^5 cells/well. After cultured for 24 h, the cells were stimulated with CAVAP-II (125, 200 and 250 μg/mL) or LPS (1 μg/mL) for another 24 h. Then, the cells were washed with cold PBS twice and then scraped into cold PBS. After centrifugation at 425*g* at 4 °C for 5 min, the resulting cell pellets were reserved and resuspended

in RIPA lysis buffer on ice for 40 min to extract the proteins. During lysis, vigorous vortex was performed every 10 min to make complete lysis. Afterwards, the samples were centrifuged at 4 °C at 15,294*g* for 20 min and the resulting supernates were carefully collected for future research. BCA kit was used to determine the protein concentration with the standard curve produced by BSA. Then 40 μg denatured proteins equilibrated with 1 × loading buffer were separated on 10% sodium dodecyl sulfate polyacrylamide gel electrophoresis (SDS-PAGE), and then transferred into PVDF membranes. Afterwards, the PVDF membranes were blocked with 5% BSA in 1 × TBS containing 0.1% Tween-20 for 1 h at room temperature with gentle shaking. Furthermore, the blots were incubated with targeted monoclonal antibodies including p-ERK1/2 (extracellular signal-regulated kinase), p-JNK (c-Jun N-terminal kinase), p-P38, p-P65 and GAPDH diluted in 5% BSA overnight at 4 °C. Subsequently, the blots were incubated with horseradish peroxidase-conjugated *anti*-rabbit IgG for 1 h at room temperature. Of note, each step above was followed with washing the membranes three times with 1 × TBST (0.1% Tween-20 in 1 × TBS) for 10 min each. The bands were finally detected using ECL Detection Kit and photographed using Molecular Image Chemi Doc XRS+ Imaging system. GAPDH was used to normalize the relative band intensity.

2.5. Statistical analysis

The data resulting from at least three separate experiments, were presented as means ± standard deviation. The statistical significance was determined using variance analysis followed by the Tukey post hoc test. $p < 0.05$ was considered as the level of significant, and $p < 0.01$ was accepted as highly significant.

3. Results

3.1. Extraction and purification of CAVAP-I and CAVAP-II

The procedures for preparation of CAVAP-I and CAVAP-II from blossoms of CAVA were summarized in Fig. 1. The yield of CAVAPs was determined to be 3.2% according to our previous reports (Shen et al., 2017). In the current experiment, two independent fractions, CAVAP-fr.1 and CAVAP-fr.2, were collected by a DEAE-Sepharose Fast Flow chromatography (Fig. 2A). Furthermore, two single and symmetrically sharp peaks (CAVAP-I and CAVAP-II) were obtained by the Sephadex G-100 chromatography and showed in Fig. 2B and C. Then CAVAP-I and CAVAP-II were kept in a sealed container for future research use after concentration, dialysis and lyophilization.

3.2. Characterization of CAVAP-I and CAVAP-II

3.2.1. Total sugar, protein and uronic acid analyses of CAVAP-I and CAVAP-II

The chemical components of CAVAP-I and CAVAP-II were summarized and listed in Table S2. The polysaccharide contents of CAVAP-I and CAVAP-II ranged from 83.15% to 77.39%. However, small amount of proteins were detected in CAVAP-I (1.28%) and CAVAP-II (0.41%). Meanwhile, the uronic acids in CAVAP-I and CAVAP-II were determined as 12.33% and 12.78%, respectively, indicating that CAVAP-I as well as CAVAP-II was acidic polysaccharide.

3.2.2. SEM analysis of CAVAP-I and CAVAP-II

The SEM images presented in Fig. 2D demonstrated that CAVAP-I and CAVAP-II showed different characteristic structures with the magnifying power of 500×, 1000× and 2000×. CAVAP-II aggregates presented mainly slice shape and smooth surface. However, CAVAP-I showed a rough and rugged surface distributed with plenty of small pores. Therefore, CAVAP-I was different from CAVAP-II in stereostructures. Additionally, the SEM analysis showed that the molecules of CAVAP-I and CAVAP-II were not closely arranged, suggesting that the interaction forces between CAVAP-I and CAVAP-II aggregates were not strong (Li et al., 2014).

3.2.3. Molecular weight determination of CAVAP-I and CAVAP-II

The average molecular weights of CAVAP-I and CAVAP-II were determined through HPGPC as demonstrated in Fig. 2F–G. Two symmetrical single peaks were observed, indicating that both CAVAP-I and CAVAP-II were possible homogeneity. Nevertheless, HPGPC could not absolutely eliminate the possibility that different polysaccharides with the same dynamical volume may co-elute in one peak (Dong et al., 2010). The average molecular weight of CAVAP-I as well as CAVAP-II was determined to be 10.5 kDa and

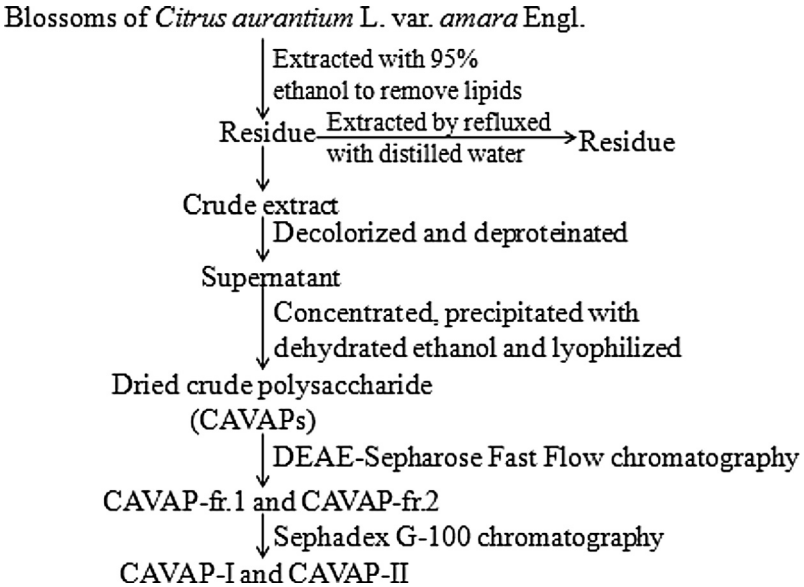

Fig. 1. Extraction and purification of CAVAP-I and CAVAP-II from blossoms of CAVA.

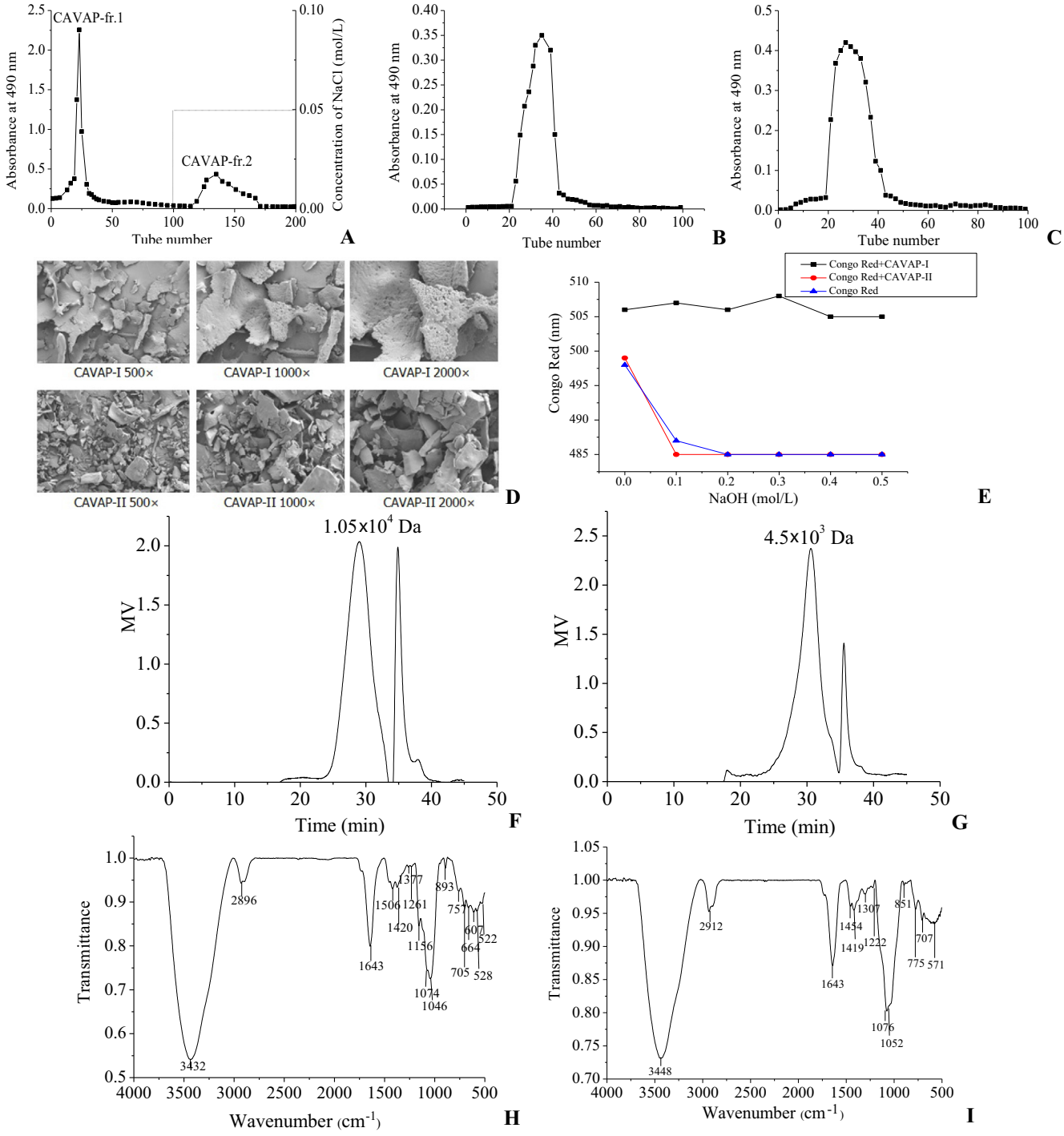

Fig. 2. Chromatography of the polysaccharides from blossoms of CAVA by DEAE-Sepharose Fast Flow chromatography (A); Chromatography of CAVAP-I (B) and CAVAP-II (C) by Sephadex G-100; scanning electron micrographs of CAVAP-I and CAVAP-II (D), triple helical conformation analysis of CAVAP-I and CAVAP-II (E), HPGPC of CAVAP-I (F) and CAVAP-II (G), FTIR spectrum of CAVAP-I (H) and CAVAP-II (I).

4.5 kDa, respectively. Obviously, CAVAP-I and CAVAP-II were lower molecular weight polysaccharides for the reason that the molecular weight of most polysaccharides generally could reach to hundreds of thousands of Da. In fact, CAVAP-II was a much lower molecular weight polysaccharide compared with CAVAP-I.

3.2.4. FT-IR spectra of CAVAP-I and CAVAP-II

In the FT-IR spectra of CAVAP-I (Fig. 2H) and CAVAP-II (Fig. 2I), most of the functional groups could be assigned according to the published literatures (Gong et al., 2015; Li et al., 2015; Zhang et al., 2016). The intense and broad bands at 3432 cm^{-1} and 3448 cm^{-1} of CAVAP-I and CAVAP-II, respectively, corresponded to the OH stretching vibrations of hydroxyl groups and those 2896 cm^{-1} and 2912 cm^{-1} were characteristic of C—H stretching vibrations of CH_2 groups. The bands at 1643 cm^{-1} and 1420 cm^{-1} of CAVAP-I and those at 1643 cm^{-1} and 1419 cm^{-1} of CAVAP-II represented the asymmetric and symmetric stretching vibrations of carboxyl groups or carboxylate, indicating that both CAVAP-I and CAVAP-II were acidic polysaccharides. The results were consistent with the uronic acid contents obtained in 3.2.1. Furthermore,

the strong bands of CAVAP-I and CAVAP-II centered at 1420 cm^{-1} and 1419 cm^{-1}, respectively, arose from the C=C stretching vibration and their strong peaks at 1046 cm^{-1} and 1052 cm^{-1} were ascribed to the stretching vibrations of pyranose ring. The characteristic absorptions at 893 cm^{-1} of CAVAP-I and 851 cm^{-1} of CAVAP-II were also observed, suggesting the β-pyranoside linkage of the glucosyl residue. At the same time, the bands of CAVAP-I and CAVAP-II at 757 cm^{-1} and 775 cm^{-1}, respectively, indicated the β-pyranoside form of the mannose residue. Eventually, the absorption peaks at 528 cm^{-1} of CAVAP-I and 571 cm^{-1} of CAVAP-II indicated the presence of α-configurations. Therefore, the spectra indicated that CAVAP-I and CAVAP-II had the typical groups of sugars.

3.2.5. Conformational structure of CAVAP-I and CAVAP-II

Polysaccharides are generally considered to exist in a triple-stranded helical conformation. Therefore, Congo red method was applied to identify the triple-stranded helical conformation of CAVAP-I and CAVAP-II. As shown in Fig. 2E, the bathochromic shift from 498 to 506 nm of the maximum absorption wavelength was an indicator of complexation of Congo red and CAVAP-I. However, the maximum absorption values did not show dramatic changes with the increase of NaOH concentrations, suggesting that CAVAP-I did not exhibit a triple helical conformation (Wang et al., 2016). The result was similar to that of MC-1 which was isolated from the root of *L. meyenii* (Zhang et al., 2016). One possible explanation would be that CAVAP-I had another order conformation which could form a stable complex with Congo red in NaOH solutions (Zhang et al., 2016). Simultaneously, the shift from 498 to 499 nm of maximum absorption wavelength indicated that CAVAP-II formed a complex with Congo red. And the significant decrease of maximum absorption wavelength with the increase of NaOH concentrations suggested that the triple-helix conformation of CAVAP-II translated into single coil conformation (Li et al., 2015). The results above justified the presence of triple-stranded helical conformation in CAVAP-II. In conclusion, the conformations were quite different between CAVAP-I and CAVAP-II, which might lead to different bioactivities.

3.2.6. Monosaccharide composition of CAVAP-I and CAVAP-II

Quantitative monosaccharide analyses of CAVAP-I and CAVAP-II were performed using GC. The results shown in Fig. 3A (monosaccharide standard), Fig. 3B (CAVAP-I) and Fig. 3C (CAVAP-II) demonstrated the presence of arabinose, mannose, glucose and galactose in CAVAP-I and CAVAP-II at a molar ratio of 9.003:1.963:34.63:54.404 and 42.845:2.467:19.207:35.481, respectively. The results indicated that CAVAP-I as well as CAVAP-II was a kind of heteropolysaccharide. Furthermore, the data suggested that galactose and arabinose accounted for the greatest proportion of CAVAP-I and CAVAP-II, respectively. Although CAVAP-I and CAVAP-II were composed of same kinds of monosaccharides, significant differences were showed in their percent contents.

3.2.7. Periodate oxidation-smith degradation of CAVAP-I and CAVAP-II

The monosaccharide and standard substance mixture was investigated to determine the glycosidic linkages of CAVAP-I and CAVAP-II. Firstly, periodate oxidation analysis demonstrated that the consumption of periodate (0.2701 mol) by 1 mol of sugar residue was more than two times of the production of formic acid (0.1021 mol), indicating that one or more of (1 → 6), (1 → 2) or (1 → 4)-linked glycosidic bonds might exist. Then, CAVAP-I and CAVAP-II were further analyzed by Smith degradation. Glycerol, glycol, phycite, arabinose, mannose, glucose and galactose were observed in CAVAP-I and CAVAP-II after Smith degradation (Fig. 3D–F). Glycerol corresponded to the appresence of (1 → 2) or (1 → 6)-linked glycosidic bonds. The appearance of erythritol indicated the existence of (1 → 4)-linked glycosidic bonds. Additionally, the presence of monosaccharides (arabinose, mannose, glucose and galactose) implied the existence of (1 → 3)-linked glycosidic bonds. Methylation analysis was carried out in order to confirm more precise glycosidic bonds.

3.2.8. Methylation analysis of CAVAP-I and CAVAP-II

Methylation analysis was employed to obtain more structural information on CAVAP-I and CAVAP-II. According to the retention time, the peaks of both CAVAP-I and CAVAP-II were identified as 2,3-Me_2-Ara*f*, 2,4-Me_2-Man*p*, 2,3,4,6-Me_4-Glc*p*, 2,3,6-Me_3-Glc*p*, 2,4-Me_2-Gal*p* and 2,3,4-Me_3-Gal*p* with different molar ratios of 13.18: 2.94: 19.44: 9.55: 37.17: 17.72 and 58.59: 7.69: 2.93: 7.24: 1.25: 22.30, respectively (Table 1). The result suggested that CAVAP-I and CAVAP-II contained six linkage forms: (1 → 5)-linked arabinose, (1 → 3,6)-linked mannose, (1 →)-linked glucose, (1 → 4)-linked glucose, (1 → 3,6)-linked galactose and (1 → 6)-linked galactose. These inferences also agreed with the results from the periodate oxidation-Smith degradation in 3.2.7. The ratio between branching points (1,3,6-Man*p* and 1,3,6-Gal*p*) and the terminal units (T-Glc*p*) of CAVAP-I was 2.06, indicating that the number of branching points was much more than that of terminal units. These results indicated that CAVAP-I contained the linear and branched polysaccharides, and the branched polysaccharides were approximately twice as much as the linear polysaccharide. In addition, the degree of branching (DB) value of CAVAP-I was calculated as 59.55% following the equation:

$$DB = (NT + NB)/(NT + NB + NL) \quad (1)$$

where NT, NB and NL represented the number of the terminal residues (T-Glc*p*), branch residues (1,3,6-Man*p* and 1,3,6-Gal*p*) and linear residues (1,5-Ara*f*, 1,4-Glc*p* and 1,6-Gal*p*), respectively.

Simultaneously, CAVAP-II was also considered to contain the linear and branched polysaccharides and its DB value was determined as 11.87%. Above all, monosaccharide composition and methylation analysis demonstrated that (1 → 3, 6)-linked galactose and (1 → 5)-linked arabinose were the largest amount of residues in CAVAP-I and CAVAP-II, respectively.

3.2.9. NMR analysis of CAVAP-I and CAVAP-II

The structural features of CAVAP-I and CAVAP-II were further identified by NMR spectral analysis and their spectra of ^{13}C NMR and ^{1}H NMR were shown in Fig. 4A–D. The anomeric carbon signals (δ 106.71, 103.90, 99.78, 101.22, 106.71 and 103.40) of CAVAP-I in Fig. 4A corresponded with H-1 and C-1 of six anomeric residues ((1 → 5)-α-L-Ara, (1 → 3,6)-α-L-Man, (1 →)-β-D-Glc, (1 → 4)-β-D-Glc, (1 → 3,6)-β-D-Gal and (1 → 6)-β-D-Gal). As for CAVAP-II, the chemical shifts of anomeric carbons at 107.45, 97.39, 100.75, 101.46, 103.43 and 103.17 ppm (Fig. 4C), and those of anomeric protons at 5.16, 4.40, 5.02, 5.00, 4.42 and 4.41 ppm (Fig. 4D), were identified as (1 → 5)-α-L-Ara, (1 → 3,6)-α-L-Man, (1 →)-α-D-Glc, (1 → 4)-β-D-Glc, (1 → 3,6)-β-D-Gal and (1 → 6)-β-D-Gal, respectively. The entire assignments of the ^{13}C and ^{1}H chemical shifts for CAVAP-I and CAVAP-II were compared with the previous literatures and illustrated in Table S3 (Niu et al., 2014; Senchenkova et al., 2014; Tian, Zhao, Zeng, Zhang, & Zheng, 2016; Zhang et al., 2016). In summary, the NMR data showed that CAVAP-I differed from CAVAP-II in the molar ratios of glucosidic bonds.

3.3. Immunomodulatory activity of CAVAP-I and CAVAP-II

We previously reported that CAVAPs exerted immunostimulatory effects through activating MAPKs and NF-κB signaling

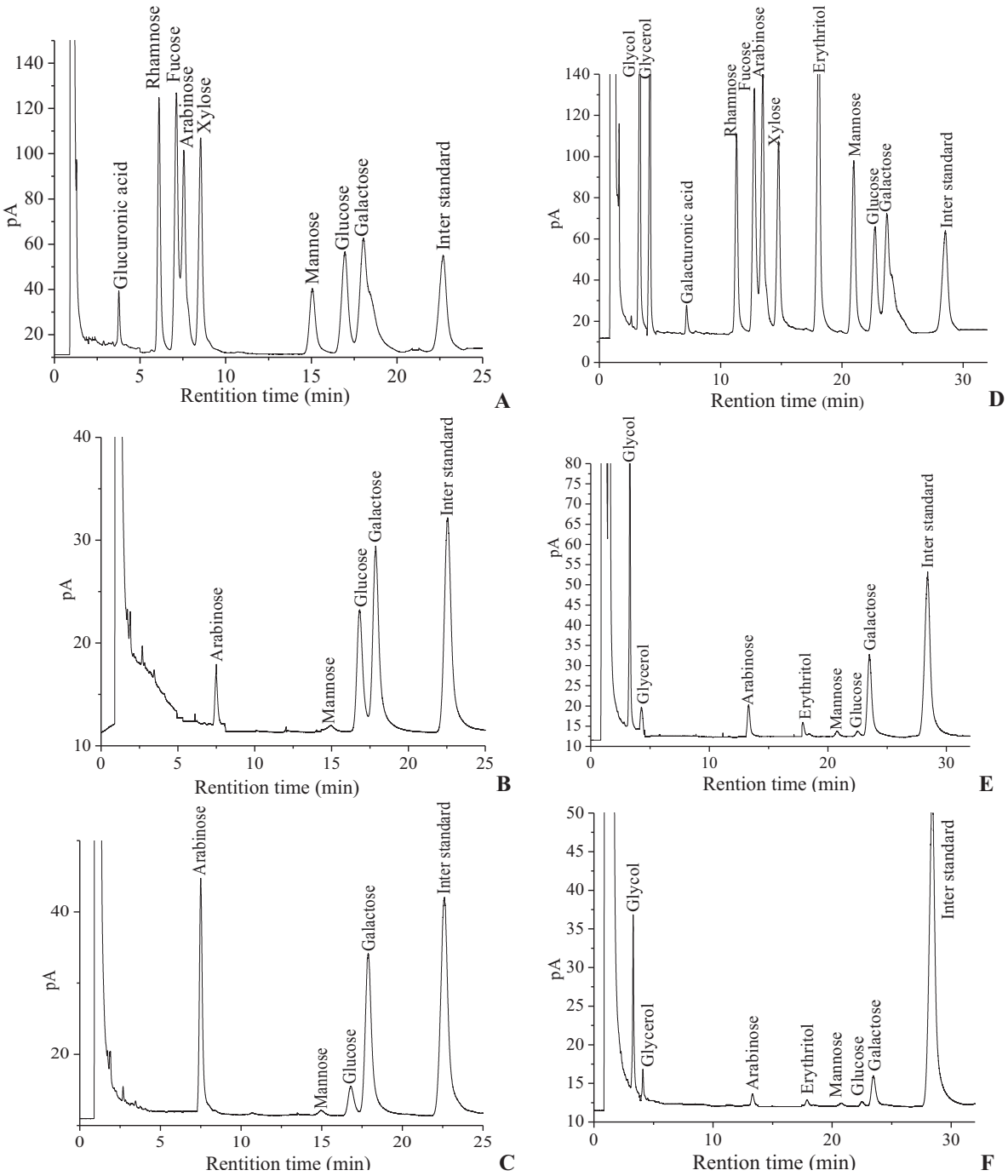

Fig. 3. Ion-exchange chromatography of the monosaccharide mixture (A), CAVAP-I (B), CAVAP-II (C); GC chromatography of the standard substance mixture (D), CAVAP-I (E), CAVAP-II (F) after Smith degradation.

Table 1
Glycosidic linkage composition of methylated CAVAP-I and CAVAP-II.

Retention time (min)	Methylated sugar	Linkage	Molar ratio (%)	
			CAVAP-I	CAVAP-II
6.390	2,3-Me_2-Ara*f*	1,5-	13.18	58.59
12.115	2,4-Me_2-Man*p*	1,3,6-	2.94	7.69
7.089	2,3,4,6-Me_4-Glc*p*	T-	19.44	2.93
9.220	2,3,6-Me_3-Glc*p*	1,4-	9.55	7.24
9.231	2,4-Me_2-Gal*p*	1,3,6-	37.17	1.25
10.504	2,3,4-Me_3-Gal*p*	1,6-	17.72	22.30

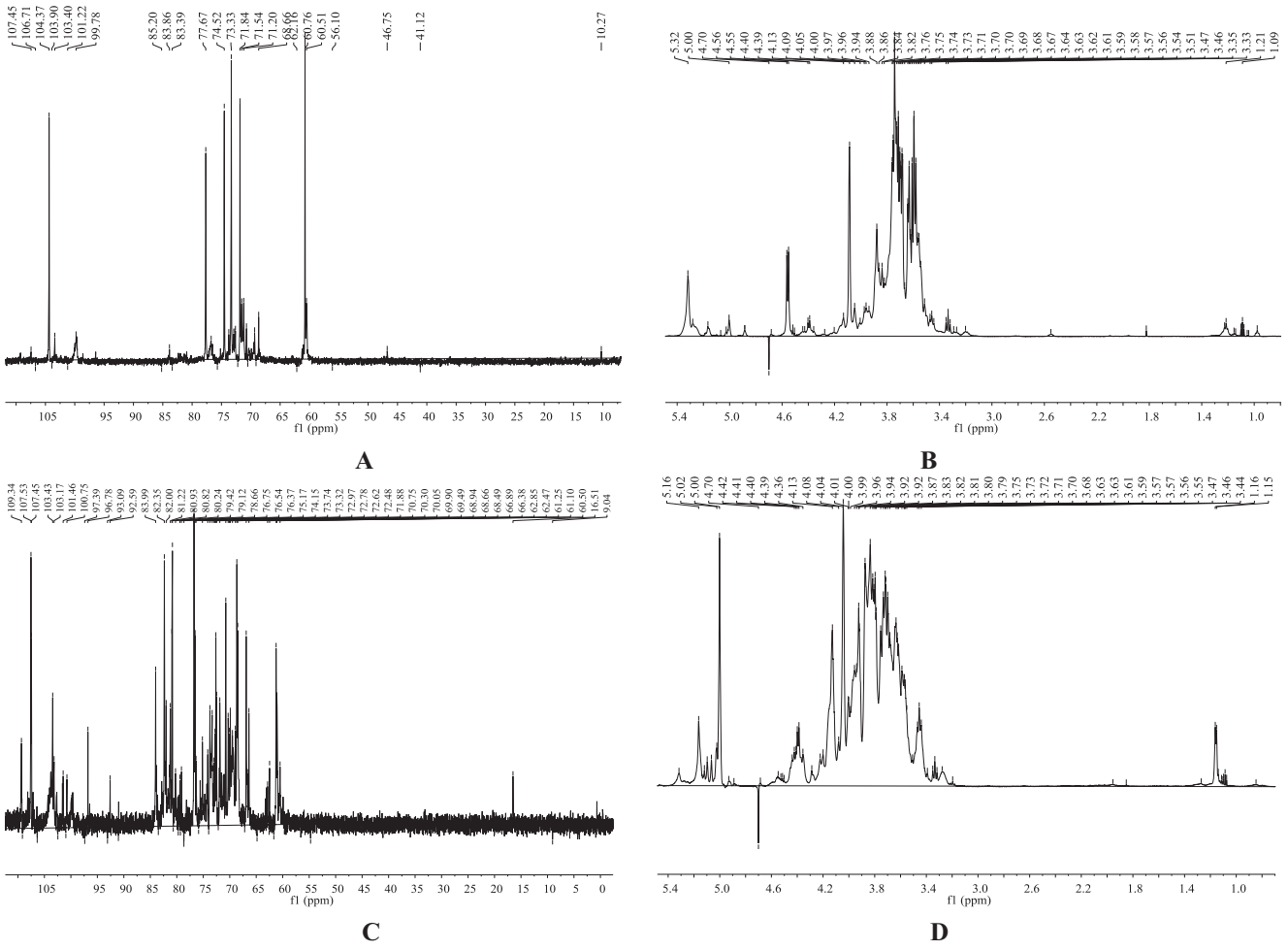

Fig. 4. ^{13}C NMR (A) and ^{1}H NMR (B) spectra of CAVAP-I, ^{13}C NMR (C) and ^{1}H NMR (D) spectra of CAVAP-II.

pathways thereby up-regulating the secretion of cytokines and genes in RAW264.7 cells. In this study, we further explored the immune enhancement effects of purified polysaccharides (CAVAP-I and CAVAP-II) from CAVAPs.

3.3.1. Effects of CAVAP-I and CAVAP-II on production of NO, IL-6 and TNF-α

CAVAP-I and CAVAP-II exhibited no cytotoxicity (data not shown) towards RAW264.7 cells at concentrations varying from 16.13 to 250 μg/mL. Thus, concentrations of 16.13, 31.25, 62.5, 125, 200 and 250 μg/mL were set as working concentrations for further researches. As shown in Fig. 5A, RAW264.7 visibly increased in size and became irregular in shape compared with the normal control group after treated with CAVAP-I or CAVAP-II for 24 h, indicating that macrophages were activated. The result was consistent with that of CAVAPs (Shen et al., 2017). Moreover, RAW264.7 cells treated with CAVAP-I or CAVAP-II produced more NO than that of control cells. Specifically, NO accumulation of RAW264.7 cells pre-treated with CAVAP-II at 16.13 μg/mL was increased to 17.44 ± 0.4 and exceeded that of LPS group (15.38 ± 0.5) (Fig. 5B). Obviously, CAVAP-II significantly stimulated more NO secretion than that of CAVAP-I. Therefore, CAVAP-II was used for further research to clarify its molecular mechanism. Compared with our previous report, it could infer that CAVAP-II at 16.13 μg/mL might exert better immunomodulatory effect than CAVAPs at 500 μg/mL, indicating that CAVAP-II might be applied as a novel immunomodulatory agent even at low concentrations (Shen et al., 2017).

3.3.2. Effects of CAVAP-II on expression of iNOS, IL-6, TNF-α and IL-1β

ELISA and RT-PCR methods were applied to detect the expression of iNOS, IL-6, TNF-α and IL-1β in order to further confirm and explain the results obtained above. Accumulation of IL-6 (Fig. 5C) as well as TNF-α (Fig. 5D) was significantly increased in a dose-dependent manner when RAW264.7 cells were incubated with CAVAP-II at 31.25, 62.5, 125, 200 and 250 μg/mL. However, production of IL-6 and TNF-α decreased sharply when CAVAP-II was up to 250 μg/mL. Furthermore, gene expression levels of iNOS (Fig. 5E), IL-6 (Fig. 5F) and TNF-α (Fig. 5G) were all significantly increased in a concentration-dependent manner when administrated with CAVAP-II ranging from 31.25 to 250 μg/mL. Additionally, CAVAP-II (31.25–250 μg/mL) brought hundreds of folds increase in gene expression levels of IL-1β (Fig. 5H), compared with the control group. The expression levels of IL-1β in the control group, LPS group and CAVAP-II group were 1.0 ± 0.38, 804.60 ± 25.45, 1211.00 ± 29.20, 1075.00 ± 28.24, 943.19 ± 34.23, 899.91 ± 24.59 and 878.57 ± 22.80, respectively. Of note, IL-1β expression levels exceeded the positive control of LPS (1 μg/mL) although they decreased with the increase of CAVAP-II concentration. In conclusion, CAVAP-II might up-regulate the production of NO, IL-6 and TNF-α through promoting the gene expression of iNOS, IL-6 and TNF-α, similarly to the effect of CAVAPs (Shen et al., 2017).

3.3.3. Effects of CAVAP-II on MAPKs and NF-κB signaling pathways

MAPKs and NF-κB signaling pathways are known to be involved in the production of cytokines in response to a variety of stimuli

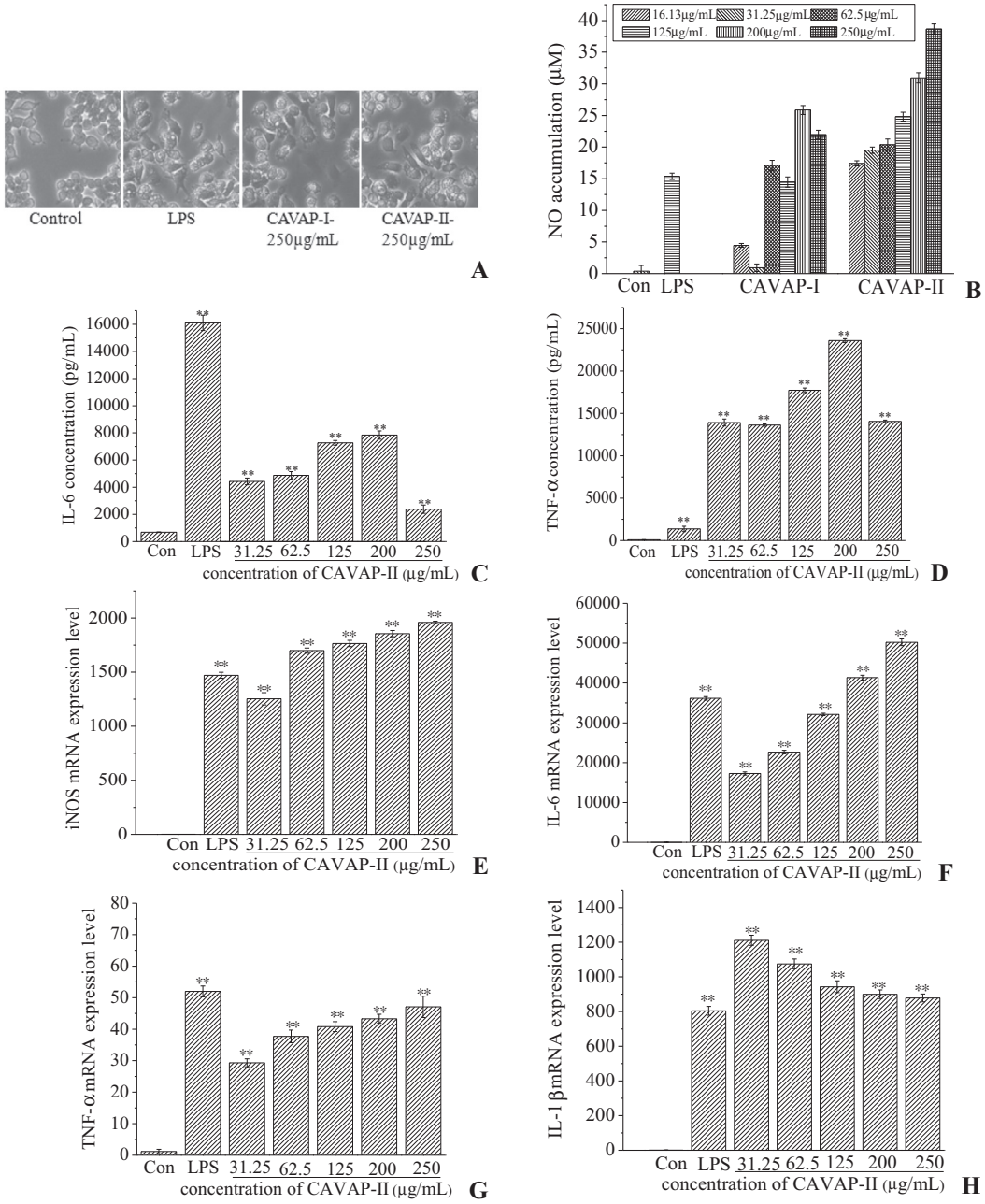

Fig. 5. Pictures of RAW264.7 cells by an invert microscope after treated with CAVAP-I and CAVAP-II (A); Effect of CAVAP-I and CAVAP-II on production of NO (B); Effect of CAVAP-II on secretion of IL-6 (C) and TNF-α (D); Effect of CAVAP-II on mRNA expression levels of iNOS (E), IL-6 (F), TNF-α (G), IL-1β (H). All experiments were run in triplicate, and data showed mean ± SD values. $^{*}p < 0.05$ and $^{**}p < 0.01$ compared to control group.

(Hayden & Ghosh, 2008). Reportedly, polysaccharides (extracted from fermented foods and edible plant extracts) could activate macrophages through triggering phosphorylation within MAPKs and NF-κB signaling pathways (Kim et al., 2013; Lee et al., 2013). To examine the underlying signaling mechanism by which CAVAP-II stimulated the gene expression of iNOS, IL-6, TNF-α and IL-1β, Western blot analysis was conducted to detect the expression of MAPK proteins, including phosphorylated-ERK, phosphorylated-JNK and phosphorylated-P38. As shown in Fig. 6, phosphorylated-ERK (Fig. 6A), phosphorylated-JNK (Fig. 6B) and phosphorylated-P38 (Fig. 6C) in RAW264.7 cells stimulated with CAVAP-II all markedly increased in a dose-dependent manner. The ratios of protein content between phosphorylated-ERK and GAPDH was 0.55 ± 0.02, 0.66 ± 0.01 and 0.78 ± 0.03 when CAVAP-II was at 125, 200 and 250 μg/mL, and the ratios of the control and LPS group were 0.22 ± 0.01 and 0.54 ± 0.02, respectively. After stimulation with CAVAP-II (125, 200, 250 μg/mL), the protein content between phosphorylated-JNK and GAPDH increased from 0.74 ± 0.03 to 1.25 ± 0.04. Moreover, the ratios of protein content between phosphorylated-P38 and GAPDH also significantly arose from 0.59 ± 0.03 to 0.91 ± 0.03 when treated with CAVAP-II at 125, 200 and 250 μg/mL. Additionally, CAVAP-II was found to induce the phosphorylation of P65 in a concentration-dependent manner (Fig. 6D), suggesting that NF-κB signaling pathway was also involved in the immune enhancement effect exerted by CAVAP-II. Above all, the results showed a dose-dependent increase of ERK1/2, JNK1/2, P38 and P65 phosphorylation, indicating that MAPKs and NF-κB signaling pathways were closely associated with

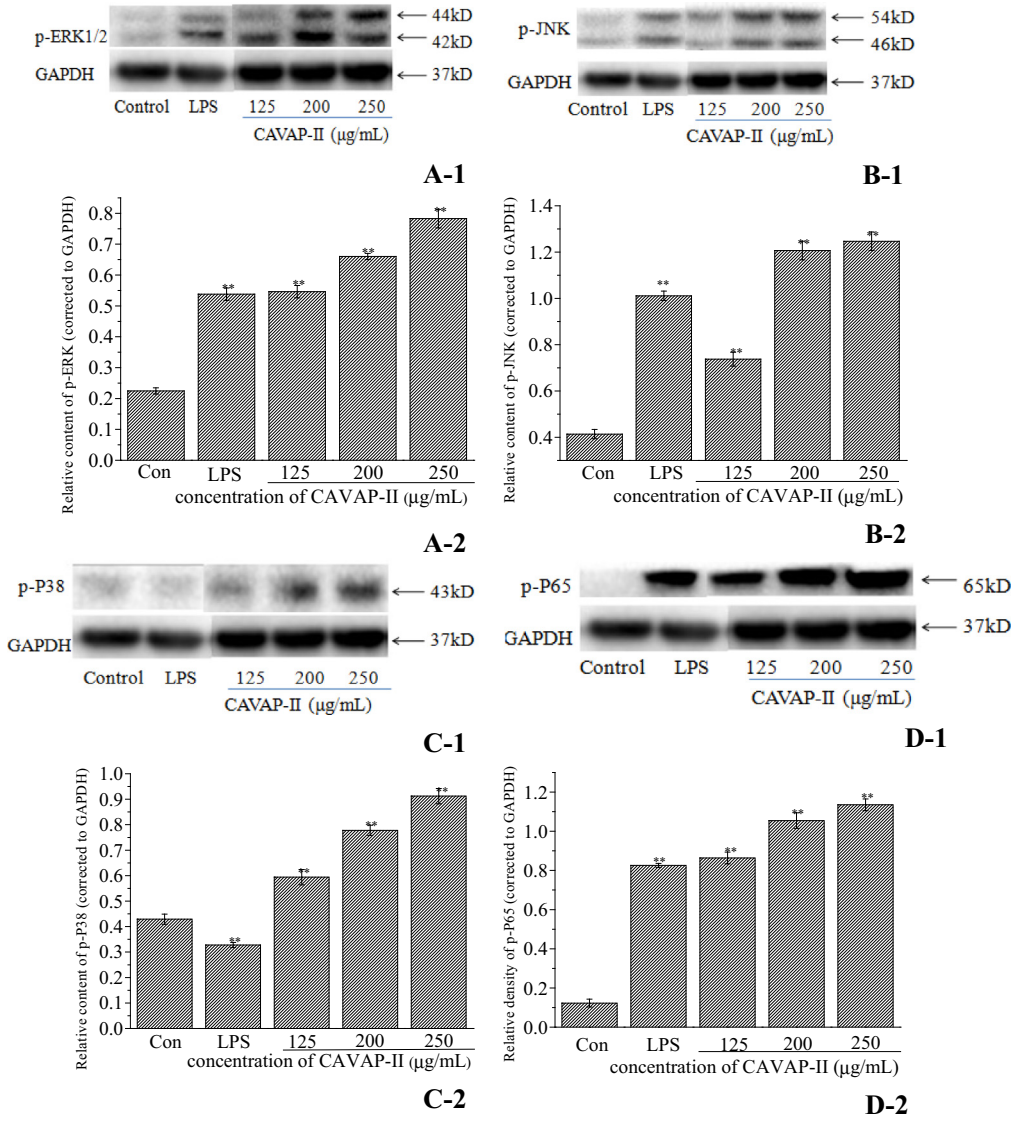

Fig. 6. Effects of CAVAP-II on the phospho-ERK1/2 (A), phospho-JNK (B), phospho-P38 MAPK (C) and phospho-P65 (D). All experiments were run in triplicate, and data showed mean ± SD values. $^{*}p < 0.05$ and $^{**}p < 0.01$ compared to control group.

macrophages activation by CAVAP-II. It concluded that CAVAP-II might exert immune enhancement effects similarly to CAVAPs.

4. Discussion

Previous study demonstrated that CAVAPs significantly activated RAW264.7 cells, indicating their strong immune enhancement effects (Shen et al., 2017). In order to further study the relationship between the structures and immunomodulatory activities of polysaccharide, CAVAP-I and CAVAP-II with molecular weight of about 10.5 kDa and 4.5 kDa, respectively, were purified from blossoms of CAVA by DEAE-Sepharose Fast Flow column chromatography and Sephadex G-100 chromatography. Then we investigated the structural characteristics including differences of CAVAP-I and CAVAP-II. Total sugars, proteins and uronic acids contents, as well as FT-IR spectra were similar between CAVAP-I and CAVAP-II. However, the SEM analysis revealed that CAVAP-I and CAVAP-II produced different stereostructures. Moreover, Congo red analysis indicated that CAVAP-II exhibited a triple helical conformation, which might be responsible for the significant immunomodulatory activity. In support, polysaccharides with the triple helical conformation generally possessed potent immunomodulatory effects (Devi et al., 2013; Satitmanwiwat et al., 2012).

Reportedly, many factors were involved in the activities of polysaccharides, including molecular weight, chain conformation, monosaccharide composition and glycosidic bonds (Bao, Liu, Fang, & Li, 2001; Ferreira et al., 2015). CAVAP-II was a much lower molecular weight polysaccharide compared with CAVAP-I, indicating that CAVAP-II might possess some properties different from CAVAP-II (Zhang et al., 2016). In support, Kakutani et al. demonstrated that the immune enhancement effect of glycogen was closely related to its molecular size (Kakutani et al., 2007). Simultaneously, previous study demonstrated that polysaccharides containing arabinose, mannose, glucose or galactose might have close contact with the immunomodulatory activity (Figueiredo, Bittencourt, Lopes, Sassaki, & Barreto-Bergter, 2012; Liao et al., 2015; Zhang et al., 2016). Monosaccharide composition analysis in the current study demonstrated that arabinose, mannose, glucose and galactose mainly presented in CAVAP-II, which might explain its immunomodulatory activity. Additionally, the glycosidic bonds in polysaccharides, such as the α-(1 → 5)-Ara,

α-(1→)-Glc, and β-(1 → 6)-Gal, were also reportedly to contribute to the immunomodulatory activity (Zhang et al., 2016). Also, CAVAP-II possessed these glycosidic bonds. The main linkage types of CAVAP-II were considered to be (1 → 5)-α-L-Ara, (1 → 3,6)-α-L-Man, (1→)-α-D-Glc, (1 → 4)-β-D-Glc, (1 → 3,6)-β-D-Gal and (1 → 6)-β-D-Gal based on periodate oxidation-Smith degradation, methylation analysis and NMR analysis.

CAVAP-II differed from CAVAP-I in molecular weight, chain conformation, monosaccharide composition and glucosidic bond. Meanwhile, the experiments *in vitro* displayed that CAVAP-II exhibited better immune enhancement activity than CAVAP-I, which might be due to different structures. The results suggested that the structures were extremely important in the biological activities of polysaccharides. Furthermore, ELISA kit, RT-PCR and western blotting analyses demonstrated that the immunomodulatory effect exerted by CAVAP-II might be mediated by activating MAPKs and NF-κB signaling pathways thus inducing the expression of some cytokines. These pathways will be characterized in our future study. Therefore, these results justified that CAVAP-II showed the greatest immunostimulation potential followed by CAVAP-I and CAVAPs by activating RAW264.7 cells. Also, the study provided certain theoretical guidance for further research on the structure–activity relationship and potential practical applications of CAVAP-II in the food industry.

Acknowledgment

This research was supported by Science and Technology Project of Guangzhou City (201604020150), Science and Technology Project of Guangdong (2014A020212682), Special Research of Traditional Chinese Medicine Hospital of Guangdong Province (YN2014ZH02).

Appendix A. Supplementary material

Supplementary data associated with this article can be found, in the online version, at http://dx.doi.org/10.1016/j.jff.2017.05.055.

References

Bao, X. F., Liu, C. P., Fang, J. N., & Li, X. Y. (2001). Structural and immunological studies of a major polysaccharide from spores of Ganoderma lucidum (Fr.) Karst. *Carbohydrate Research, 332*(1), 67–74.

Bradford, M. M. (1976). A rapid and sensitive method for the quantitation of microgram quantities of protein utilizing the principle of protein-dye binding. *Analytical Biochemistry, 72*, 248–254.

Devi, K. S. P., Roy, B., Patra, P., Sahoo, B., Islam, S. S., & Maiti, T. K. (2013). Characterization and lectin microarray of an immunomodulatory heteroglucan from Pleurotus ostreatus mycelia. *Carbohydrate Polymers, 94*(2), 857–865.

Dong, Q., Liu, X., Yao, J., Dong, X., Ma, C., Xu, Y., & Ding, K. (2010). Structural characterization of a pectic polysaccharide from Nerium indicum flowers. *Phytochemistry, 71*(11–12), 1430–1437.

Fang, Q., Wang, J. F., Zha, X. Q., Cui, S. H., Cao, L., & Luo, J. P. (2015). Immunomodulatory activity on macrophage of a purified polysaccharide extracted from Laminaria japonica. *Carbohydrate Polymers, 134*, 66–73.

Ferreira, S. S., Passos, C. P., Madureira, P., Vilanova, M., & Coimbra, M. A. (2015). Structure function relationships of immunostimulatory polysaccharides: A review. *Carbohydrate Polymers, 132*, 378–396.

Figueiredo, R. T., Bittencourt, V. C. B., Lopes, L. C. L., Sassaki, G., & Barreto-Bergter, E. (2012). Toll-like receptors (TLR2 and TLR4) recognize polysaccharides of Pseudallescheria boydii cell wall. *Carbohydrate Research, 356*, 260–264.

Gong, L., Zhang, H., Niu, Y., Chen, L., Liu, J., Alaxi, S., & Yu, L. (2015). A novel alkali extractable polysaccharide from *Plantago asiatic* L. seeds and its radical-scavenging and bile acid-binding activities. *Journal of Agricultural and Food Chemistry, 63*(2), 569–577.

Hayden, M. S., & Ghosh, S. (2008). Shared principles in NF-kappa B signaling. *Cell, 132*(3), 344–362.

Kakutani, R., Adachi, Y., Kajiura, H., Takata, H., Kuriki, T., & Ohno, N. (2007). Relationship between structure and immuno stimulating activity of enzymatically synthesized glycogen. *Carbohydrate Research, 342*(16), 2371–2379.

Kim, H. S., Kim, Y. J., Lee, H. K., Ryu, H. S., Kim, J. S., Yoon, M. J., & Han, S. B. (2012). Activation of macrophages by polysaccharide isolated from Paecilomyces cicadae through toll-like receptor 4. *Food and Chemical Toxicology, 50*(9), 3190–3197.

Kim, T. H., Lee, S. J., Rim, H. K., Shin, J. S., Jung, J. Y., Heo, J. S., & Lee, K. T. (2013). In vitro and in vivo immunostimulatory effects of hot water extracts from the leaves of Artemisia princeps Pampanini cv. Sajabal. *Journal of Ethnopharmacology, 149*(1), 254–262.

Lee, J. S., Kwon, D. S., Lee, K. R., Park, J. M., Ha, S. J., & Hong, E. K. (2015). Mechanism of macrophage activation induced by polysaccharide from Cordyceps militaris culture broth. *Carbohydrate Polymers, 120*, 29–37.

Lee, S. J., Rim, H. K., Jung, J. Y., An, H. J., Shin, J. S., Cho, C. W., & Lee, K. T. (2013). Immunostimulatory activity of polysaccharides from Cheonggukjang. *Food and Chemical Toxicology, 59*, 476–484.

Li, H., Liu, L., Tao, Y., Zhao, P., Wang, F., Huai, L., & Xu, Y. (2014). Effects of polysaccharides from Pholiota nameko on maturation of murine bone marrow-derived dendritic cells. *International Journal of Biological Macromolecules, 63*, 188–197.

Li, W., Xia, X., Tang, W., Ji, J., Rui, X., Chen, X., & Dong, M. (2015). Structural characterization and anticancer activity of cell-bound exopolysaccharide from Lactobacillus helveticus MB2-1. *Journal of Agricultural and Food Chemistry, 63*(13), 3454–3463.

Liao, W. Z., Luo, Z., Liu, D., Ning, Z. X., Yang, J. G., & Ren, J. Y. (2015). Structure characterization of a novel polysaccharide from dictyophora indusiata and its macrophage immunomodulatory activities. *Journal of Agricultural and Food Chemistry, 63*(2), 535–544.

Lu, C. L., Zhu, W., Wang, M., Hu, M. M., Chen, W. L., Xu, X. J., & Lu, C. J. (2015). Polysaccharides from Smilax glabra inhibit the pro-inflammatory mediators via ERK1/2 and JNK pathways in LPS-induced RAW264.7 cells. *Carbohydrate Polymers, 122*, 428–436.

Mao, G. H., Ren, Y., Li, Q., Wu, H. Y., Jin, D., Zhao, T., & Wu, X. Y. (2016). Anti-tumor and immunomodulatory activity of selenium (Se)-polysaccharide from Se-enriched Grifola frondosa. *International Journal of Biological Macromolecules, 82*, 607–613.

Niu, Y., Shang, P., Chen, L., Zhang, H., Gong, L., Zhang, X., & Yu, L. (2014). Characterization of a novel alkali-soluble heteropolysaccharide from tetraploid gynostemma pentaphyllum makino and its potential anti-inflammatory and antioxidant properties. *Journal of Agricultural and Food Chemistry, 62*(17), 3783–3790.

Radhakrishnamurthy, B., & Berenson, G. S. (1963). Identification of uronic acids in mucopolysaccharides. *Archives of Biochemistry and Biophysics, 101*, 360–362.

Satitmanwiwat, S., Ratanakhanokchai, K., Laohakunjit, N., Chao, L. K., Chen, S. T., Pason, P., & Kyu, K. L. (2012). Improved purity and immunostimulatory activity of beta-(1 -> 3)(1 -> 6)-Glucan from Pleurotus sajor-caju using cell wall-degrading enzymes. *Journal of Agricultural and Food Chemistry, 60*(21), 5423–5430.

Senchenkova, S. Y. N., Shashkov, A. S., Shneider, M. M., Arbatsky, N. P., Popova, A. V., Miroshnikov, K. A., & Knirel, Y. A. (2014). Structure of the capsular polysaccharide of Acinetobacter baumannii ACICU containing di-N-acetylpseudaminic acid. *Carbohydrate Research, 391*, 89–92.

Shen, C. Y., Yang, L., Jiang, J. G., Zheng, C. Y., & Zhu, W. (2017). Immune enhancement effects and extraction optimization of polysaccharides from *Cirtus aurantium* L. var. *amara* Engl. *Food & Function*, 8(2), 796–807.

Shen, C. Y., Zhang, W. L., & Jiang, J. G. (2017). Immune-enhancing activity of polysaccharides from *Hibiscus sabdariffa* Linn. via MAPK and NF-kB signaling pathways in RAW264.7 cells. *Journal of Functional Foods, 34*, 118–129.

Shen, C. Y., Zhang, T. T., Zhang, W. L., & Jiang, J. G. (2016). Anti-inflammatory activities of essential oil isolated from the calyx of *Hibiscus sabdariffa* L. *Food & Function, 7*(10), 4451–4459.

Tian, Y., Zhao, Y., Zeng, H., Zhang, Y., & Zheng, B. (2016). Structural characterization of a novel neutral polysaccharide from Lentinus giganteus and its antitumor activity through inducing apoptosis. *Carbohydrate Polymers, 154*, 231–240.

Wang, J., Li, Q., Bao, A., Liu, X., Zeng, J., Yang, X., & Lei, Z. (2016). Synthesis of selenium-containing Artemisia sphaerocephala polysaccharides: Solution conformation and anti-tumor activities in vitro. *Carbohydrate Polymers, 152*, 70–78.

Wang, Q. H., Shu, Z. P., Xu, B. Q., Xing, N., Jiao, W. J., Yang, B. Y., & Kuang, H. X. (2014). Structural characterization and antioxidant activities of polysaccharides from *Citrus aurantium* L.. *International Journal of Biological Macromolecules, 67*, 112–123.

Wang, M., Yang, X. B., Zhao, J. W., Lu, C. J., & Zhu, W. (2017). Structural characterization and macrophage immunomodulatory activity of a novel polysaccharide from Smilax glabra Roxb. *Carbohydrate Polymers, 156*, 390–402.

Wei, W., Feng, L., Bao, W. R., Ma, D. L., Leung, C. H., Nie, S. P., & Han, Q. B. (2016). Structure characterization and immunomodulating effects of polysaccharides isolated from Dendrobium officinale. *Journal of Agricultural and Food Chemistry, 64*(4), 881–889.

Zeng, Q. H., Zao, J. B., Wang, J. J., Zhang, X. W., & Jiang, J. G. (2016). Comparative extraction processes, chemical compositions and antioxidant activities of essential oils from *Cirsium japonicum* DC and *Cirsium setosum* MB. *LWT-Food Science and Technology, 68*(595–605), 1.

Zhang, W., Song, D., Xu, D., Wang, T., Chen, L., & Duan, J. (2015). Characterization of polysaccharides with antioxidant and immunological activities from Rhizoma Acori Tatarinowii. *Carbohydrate Polymers, 133*, 154–162.

Zhang, M. M., Wang, G., Lai, F. R., & Wu, H. (2016). Structural characterization and immunomodulatory activity of a novel polysaccharide from *Lepidium meyenii*. *Journal of Agricultural and Food Chemistry, 64*(9), 1921–1931.